Application of physical and numerical simulations for interpretation of peripheral coarse grain structure during hot extrusion of AA7020 aluminum alloy

Eivani, A. R.; Zhou, J.

DOI
10.1016/j.jallcom.2017.06.297

Publication date
2017

Document Version
Accepted author manuscript

Published in
Journal of Alloys and Compounds

Link to formal publication Journal of Alloys and Compounds (Elsevier): https://doi.org/10.1016/j.jallcom.2017.06.297

Application of physical and numerical simulations for interpretation of peripheral coarse grain structure during hot extrusion of AA7020 aluminum alloy

A.R. Eivani [1 *], J. Zhou [2]

[1] School of Metallurgy and Materials Engineering, Iran University of Science and Technology, Tehran, Iran

[2] Department of Biomechanical Engineering, Delft University of Technology, Mekelweg 2, 2628 CD Delft, The Netherlands

Abstract

In this research, hot compression test is used to simulate the metallurgical phenomena occurring in the peripheral part of AA7020 aluminum alloy extrudates during hot extrusion and leading to the formation of the peripheral coarse grain (PCG) structure. The temperature profiles at a tracking point in the peripheral part of extrudates are predicted using finite element method (FEM). A special thermal treatment representing the predicted thermal profiles during extrusion is designed and applied to specimens after hot-compression testing. The effects of deformation conditions, i.e., temperature and strain rate, and the subsequent special thermal treatment on the formation of coarse grains in the AA7020 alloy are investigated. The as-deformed microstructures of specimens as well as the microstructures of specimens after the special thermal treatment are examined and the average grain size and homogeneity of grain size

* Corresponding author; Email: aeivani@iust.ac.ir, Tel: +98 (0) 21 77 240 540, Fax: +98 (0) 21 77 240 480.

distribution determined. It is observed that with increasing deformation temperature or decreasing strain rate, the average recrystallized grain size increases. A fine and homogenous grain structure is obtained by increasing strain rate. According to the results of this investigation, formation of coarse grains in the periphery of the extrudate is attributed to high temperatures raised during extrusion rather than high strain rates.

Keywords: Peripheral coarse grain; Hot compression; Recrystallization; Physical simulation; Numerical simulation.

1. Introduction

Industrial-scale materials processing usually involves the application of a large production system and complex process design, which makes it quite difficult to investigate the individual metallurgical and mechanical phenomena occurring during a particular manufacturing process. Physical simulation has been recognized as an economic and effective means that allows detailed studies on these phenomena. Physical simulation of materials processing usually involves the laboratory-scale representation of thermal and mechanical conditions, to which the material is subjected in the actual manufacturing process. Small samples are used and exposed to similar thermal and mechanical profiles that the same material follows during the course of the full-scale industrial manufacturing process. If physical simulation is accurate, depending on the reliability of the input data of thermal and mechanical profiles and on the capabilities of the simulator, the results can be readily translated from the laboratory to the full-scale industrial manufacturing process. In order to perform accurate physical simulations of a metal-forming process and microstructure evolutions, care must be

taken to choose an appropriate testing technique representing the industrial metal-forming process.

In recent years, Gleeble thermomechanical simulator has been extensively used for the investigation of the physical phenomena occurring during hot-forming processes. Zhang et. al. [1], investigated the dynamic and static softening behaviors of aluminum alloys (AA1050, AA5182 and AA7075 alloys) during multi-stage hot deformation by performing interrupted isothermal hot compression tests at temperatures of 300 and 400 °C and at a strain rate of 0.5 s^{-1} on Gleeble 1500. They found that considerable dynamic softening and exceptional softening associated with a structure softening happened to both AA1050 and AA7075 alloys deformed at 400 °C. Luo et. al. [2], investigated the effects of deformation parameters on the microstructures of the 7A09 aluminum alloy deformed during isothermal compression and those after solution treatment. A low deformation temperature was recommended for preventing grains from coarsening, because a high deformation temperature contributed to the dissolution of second-phase particles and the occurrence of static recrystallization during the solution treatment subsequent to hot compression. However, there has been no study reported in the open literature on physical simulation to interpret or predict the formation of the peripheral coarse grain (PCG) structure in aluminum alloy extrusions by means of Gleeble thermomechanical simulator.

The PCG structure is a well-known defect in hot-extruded aluminum alloys and it degrades extruded products in mechanical properties such as strength, fracture toughness and stress corrosion resistance [3]. Preventing the PCG structure or decreasing its extent is of great interest for the aluminum extrusion industry [3]. The issues regarding the evolution of the grain structure of extruded aluminum alloys have

been addressed by many researchers. For example, Schikorra et al. [4], presented an experimental–numerical procedure for the prediction of the recrystallized structure in aluminum extrusions. Misiolek [5] investigated the physical response of an aluminum alloy to hot deformation, i.e., the evolution of grain structure during the extrusion process. Kikuchi et. al. [6], investigated the peripheral recrystallization in Al-Zn-Mg-Cu alloys during the extrusion process. They found that the peripheral recrystallized structure was thicker at the head and tail parts of the extrusion than at the other parts. Indeed, the thickness of the PCG structure was larger towards the tail. Zhao et. al. [7], investigated the effect of deformation speed on the microstructure and mechanical properties of the AA6063 alloy during the continuous extrusion process. These researchers and many others all agree that the issue about the formation of coarse grains in extruded aluminum alloys actually concerns the complex interplay between alloy composition and the conditions applied during extrusion and post-deformation processes.

To prevent the formation of the PCG structure, two approaches have been proposed. The first one is to adjust the chemical composition of the aluminum alloy by adding minor alloying elements such as Zr [8] and Sc [9] and allow the formation of nano-sized intermetallic compounds that act as recrystallization inhibitors. The second approach is to optimize the process parameters of extrusion, subsequent cooling and thermal treatment, if the last is applied separately. For this purpose, it is of prime importance to understand the effects of deformation conditions and post-deformation thermal treatment on the resulting grain structure. Then, a correlation between a grain structure parameter, such as the average grain size, and a process parameter representative of the mechanical condition in the peripheral part of the extrudate, such

as strain rate, may be established [10]. Theoretical studies show that the strain rates in the peripheral part of the extrudate may reach values as high as 45 s^{-1} [11]. Such high strain rates locally occurring during extrusion must result in increases in the stored energy in the material [12], which may eventually lead to the formation of the PCG structure [13]. The resulting grain structure is a large and homogenous one, where grain sizes do not vary significantly. Large grain sizes and the homogeneity of the grain structure are the two primary characteristics of the PCG structure. The homogeneity of a grain structure can be quantified in terms of grain size distribution. When a large fraction of grains have similar grain sizes, the structure is said to be a homogenous one. By contrast, if a large fraction of grains exhibit variations in size over a wide range, it is an inhomogeneous grain structure.

In the open literature, there is a lack of information on the grain size distribution in the PCG structure of extruded aluminum alloys. In addition, since the peripheral part of the extrudate is subjected to quite complex thermomechanical conditions, namely high strains, high strain rates, high temperatures and heat transfer to the ambient surrounding, it is not clear which parameter is a more responsible one for the formation of the PCG structure than the others, although all of the parameters seem to have effects.

In the present research which is an extension to a previous work of the authors [14], physical simulations were performed. A special thermal treatment that represented the actual thermal conditions in the peripheral part of the extrudate during extrusion was designed and applied to the specimens of the same material after hot-compression testing. The effects of deformation conditions on the as-deformed grain structure of the AA7020 aluminum alloy and on the grain structure after the special thermal treatment were investigated. The microstructures of specimens subjected to water quench and the

special thermal treatment that entailed post-deformation heating, followed by air cooling, were characterized in terms of the average grain size and the homogeneity of the grain structure. Based on the results obtained, the mechanical and thermal conditions that led to the formation of the PCG structure were identified, which in the end allowed the suggestions to be made to inhibit the formation of this structural defect.

2. Finite element simulations of hot extrusion

A DEFORM-3D v6.1 commercial package based on the finite element method (FEM) was used for the simulation of the hot extrusion process for the Al-4.5Zn-1Mg aluminum alloy. Extrusion process parameters used for the FEM simulations as well as the dimensions of the billet, container and die are listed in Table 1.

Table 1. Dimensions of billet and tooling and main process parameters

Billet length (mm)	750
Billet diameter (mm)	203
Container inside diameter (mm)	208
Container outside diameter (mm)	2000
Reduction ratio	16
Diameter of the round bar extrudate (mm)	48
Die bearing length (mm)	10
Initial billet, die and stem temperature (°C)	460 500 540
Ram speed (mm/s)	5 7

To save computing time, only one-sixteenth of the workpiece (i.e., the billet and extrudate) and extrusion tooling were modeled, taking advantage of their symmetry. The symmetry planes were assumed to be immobile with no material movements

across these planes. FEM Simulations were performed at initial billet temperatures of 350-550 °C and at ram speeds of 2.5, 5, 7.5. 10, 12.5 and 15 mm/s. The temperature surrounding the container and die was set at 100 °C to avoid too much heat dissipation.

The Al-4.5Zn-1Mg aluminum alloy and H13 hot-work tool steel were used as the billet and extrusion tooling materials, respectively, both in the FEM simulations and experiments. A thermo-viscoplastic material model was used for the billet and a thermo-rigid material model for the extrusion tooling. Both of these material models neglected the elastic behavior of the billet and tooling materials. The extrusion tooling was composed of die, container and stem with a dummy block on its front. The physical properties of the workpiece material and the H13 tooling material are given in Table 2.

Table 2. Physical properties of the AA7020 workpiece and H13 tooling.

Parameter	AA 7020 Aluminum	H-13 tool steel
Heat capacity (N / mm² °C)	2.4	5.6
Thermal conductivity (W / m °C)	180.2	28.4
Heat transfer coefficient between tooling and billet (N / °Csmm²)	11	11
Heat transfer coefficient between tooling / billet and air (N / °Csmm²)	0.02	0.02
Emissivity	0.7	0.7
Limiting strain rate (s^{-1})	0.0076	---

The flow stress-strain data of the AA7020 alloy were determined through hot compression tests using a Gleeble 3800 thermomechanical simulator. To take the effect of deformational heating during hot compression at high strain rates on the actual specimen temperature into account, the flow stress-strain curves obtained from these tests were corrected [15, 16]. The details of the hot compression tests and corrected flow stress-strain curves are presented elsewhere [15]. The flow stress-strain data over

a temperature range of 350 to 550 °C and a strain rate range of 0.1 to 100 s^{-1} were input into the DEFORM pre-processor.

All the extrusion tooling was meshed with tetrahedral elements and its heat exchanges with the workpiece were incorporated into the EFM simulations. FEM simulation parameters used in this research are listed in Table 3. To enhance the efficiency of the FEM simulations and to obtain specific resolutions in the areas of particular interest, a number of windows with an increased element density were applied to generate local finer elements, especially around the die orifice.

Table 3. Simulation parameters used in this research

Total number of elements	90,000
Minimum size of element (mm)	0.5
Relative interference depth	0.7
Temperature range for flow stress measurement (◦C)	350–450
Strain rate range for flow stress measurement (s^{-1})	0.01–10
Shear friction factor between billet and tooling	1.0

The minimum size of the element was 1 mm. The total number of elements was 20,000. A relative interference depth of 0.3 was defined to trigger the remeshing procedure when any element at the edge of the workpiece had been penetrated into and the penetration depth exceeded 70% of the original length of the surface edge that had a contact node at each end. The friction at the workpiece-tooling interfaces was considered to be of shear-type. The friction factor m_f $(0 \le m_f \le 1)$ was expressed as

$$m_f = \sqrt{3}\frac{\tau_s}{\sigma_e} \quad (1)$$

where τ_s is the frictional shear stress and σ_e the effective flow stress of the workpiece. A friction factor of 1.0 at the container-billet interface was chosen. The same friction factor was assumed at the interfaces between the billet and the dummy block and between the billet and the die.

3. Experimental procedure

AA7020 aluminum alloy billets had a diameter of 48 mm. The chemical composition of the billet material is shown in Table 4. For hot compression tests, the billets were extruded at 450 °C to produce bars with a diameter of 15.8 mm. The bars were machined to make cylindrical specimens with a length of 12 mm and a diameter of 10 mm. In order to eliminate the effect of deformation on the microstructure of the extruded bars, introduced during extrusion, and to obtain a homogenous structure, the specimens were annealed at 550 °C for 15 s in a salt-bath furnace. The grain structures of these specimens were examined and an average grain size of 273 μm was determined, following the general intercept procedure according to ASTM E 112-96 [17].

Table 4- Chemical compositions of the AA7020 alloy used in this study.

Element (Wt %)	Si	Fe	Cu	Mn	Mg	Zn	Ti	Cr	Zr	Al
N1	0.31	0.28	0.2	0.34	1.24	4.36	0.001	0.10	0.08	Bal.

Hot compression tests were carried out at four temperatures, i.e., 350, 400, 450, and 500 °C and at strain rates varying from 0.1 to 100 s^{-1}. 0.1 mm thick graphite plate was used for lubrication. Compression deformation proceeded to a strain of 0.6. Tests were

performed at least twice under each condition to ensure the repeatability and accuracy of data. The specimen was heated to the desired temperature at a rate of 10 °C/s and kept at the temperature for a certain period of time in order to attain a homogenous temperature in the test material and anvils. Previous studies [16] on the same Gleeble thermomechanical simulator showed that soaking time should be adapted according to the deformation temperature. In the present work, soaking time was 90 s when deformation temperature was 350 or 400 °C and 110 s when deformation temperature was 450 or 500 °C.

In this study, two batches of specimens were subjected to different thermal treatments after the compression tests. The first batch was subjected to water quenching to retain the as-deformed structure. It was intended to ensure that no further microstructural changes would occur after deformation so that the resulting microstructure exhibited deformed (unrecrystallized) and dynamically recrystallized grains.

To simulate the physical phenomena, i.e., the temperature increase that occurs to the deforming material during hot extrusion, a special thermal treatment was designed in [14] and is used in this investigation, as schematically presented in Fig. 1. It was intended to reproduce the thermal conditions occurring in the peripheral part of the extrudate. From the FEM simulation results about the temperature increases during extrusion under different conditions, an value of temperature increase, 75 °C, was considered to represent thermal conditions occurring in the peripheral part of the extrudate. The specimens were then air-cooled.

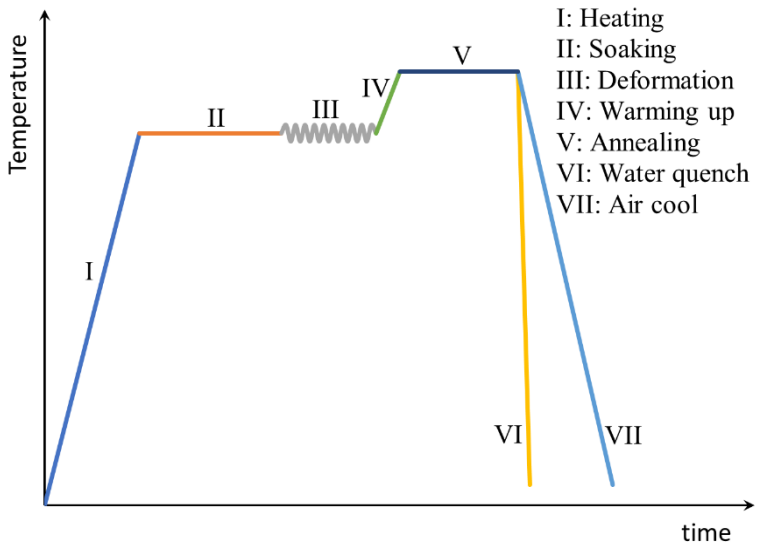

Figure 1- Special thermal treatment applied to hot-compression tested specimens for the physical simulation of the phenomena occurring in the peripheral part of the extrudate [14].

Optical microscopy was performed using Philips polarized light microscope. The longitudinal cross section of both compression test samples and the extruded rods were chosen for the investigation. The microstructures of the samples after hot compression tests are extracted from a central region at which the uniformity of deformation is guaranteed. The microstructures of the specimens after water quenching and the special thermal treatment were compared in terms of the average grain size and grain size distribution determined using the general intercept method. In addition, the recrystallized volume fraction was determined according to the ASTM E562-89 standard point counting technique [18]. The measurements were repeated to ensure accuracy and a minimum of 20 fields were analyzed.

4. Results and Discussion

4.1 Material behavior

Fig. 2 illustrates the flow stress-strain curves of the alloy at various hot compression conditions. It is clear that at a given temperature, with increasing strain rate, flow stress

increases. Comparisons between the curves at a given strain rate show that the flow stress is higher at a lower deformation temperature. It is also clear that after a strain of 0.1 is reached, the flow stress remains almost unchanged. With dynamic recovery as the dominant restoration mechanism, the steady-state flow stress is related to the subgrain size of the deformed structure [12]. It has been demonstrated by Ceri et. al. [19], that at a lower deformation temperature and higher strain rate, subgrains are expected to be finer, leading to a higher flow stress.

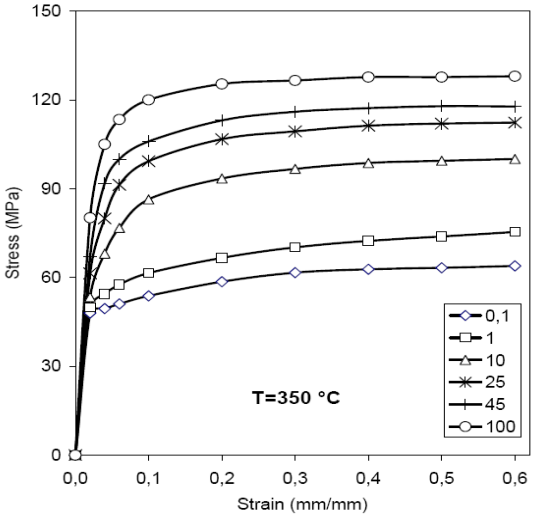

(a)

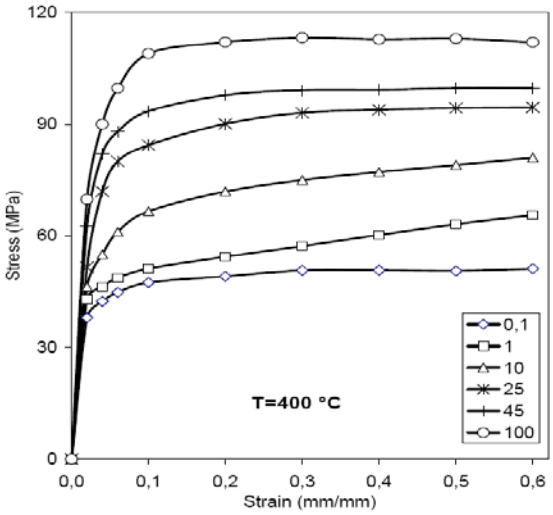

(b)

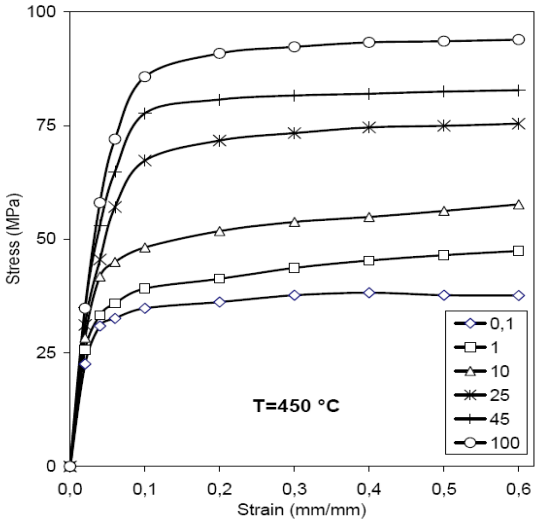

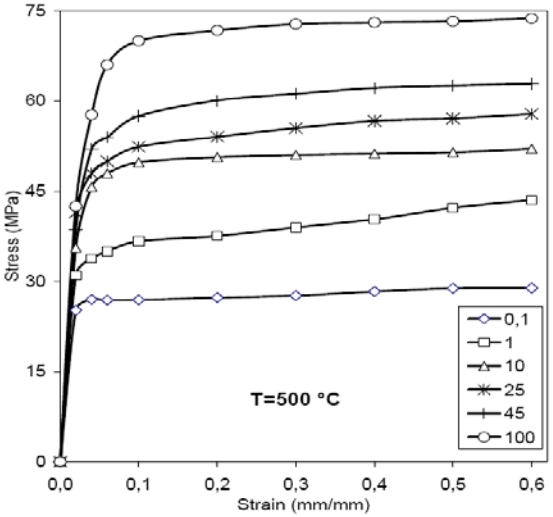

(c) (d)

Figure 2- Flow stress-strain curves of the AA7020 aluminum alloy used in this study, obtained from hot compression tests at temperatures of (a) 350, (b) 400, (c) 450 and (d) 500 °C. The unit of the strain rate is s^{-1}.

It is well established that for most of wrought aluminum alloys subgrain size is correlated with the Zener-Hollomon parameter, *Z*, which is in turn a function of strain rate and deformation temperature [3]. To calculate the Z value, the apparent activation energy for hot deformation is needed, which can be determined by using Eq. (1):

$$Z = \dot{\varepsilon} \exp\left(\frac{Q_{HW}}{R_g T_{HW}}\right) = A_Z \left(\sinh \alpha_Z \sigma_P\right)^n \quad (1)$$

where A_Z, α_Z and n are constants, R_g the universal gas constant and Q_{HW} the apparent activation energy for hot deformation. Q_{HW} can be obtained from the slope in an Arrhenius-type plot [19]:

$$Q_{HW} = 2.3 n R_g S_A \quad (2)$$

where S_A is defined as:

$$S_A = \frac{d \ln\left(\sinh \alpha_Z \sigma_P\right)}{d\left(1/T\right)} \quad (3)$$

The initial fitting was carried out in the traditional graphical manner with α = 0.052 MPa^{-1} [19] and the constant T lines in the $\log \dot{\varepsilon}$ against $\log\left(\sinh\left(\alpha\sigma\right)\right)$ plots were

constrained to be parallel with each other for the best overall fit, yielding the slope n, as shown in Fig. 3. In the plots of $\log\left(\sinh\left(\alpha\sigma\right)\right)$ against $(1/T)$, the lines of constant $\dot{\varepsilon}$ were constrained to be parallel with one another and the slope was used for the calculation of Q_{HW}, Fig. 4. The n, S_A and Q_{HW} values obtained are given in Table 5. These values are in reasonable agreement with those of a similar alloy, i.e., AA7012 in the same alloy system [19].

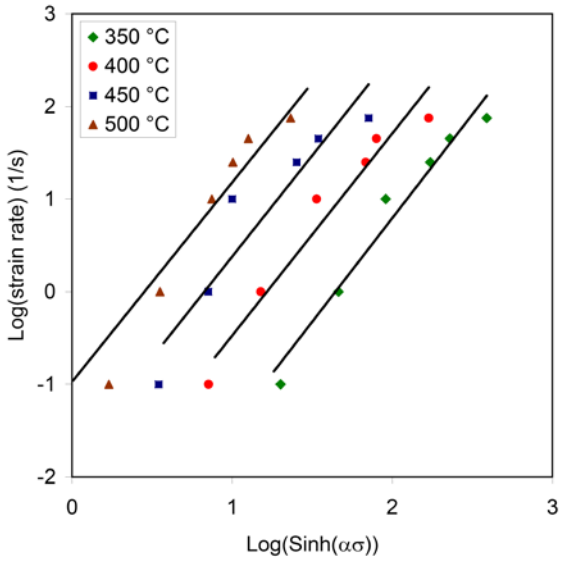

Figure 3- Plots of $\log\dot{\varepsilon}$ against $\log\left(\sinh\left(\alpha\sigma\right)\right)$ at constant temperatures with α = 0.052 MPa^{-1}.

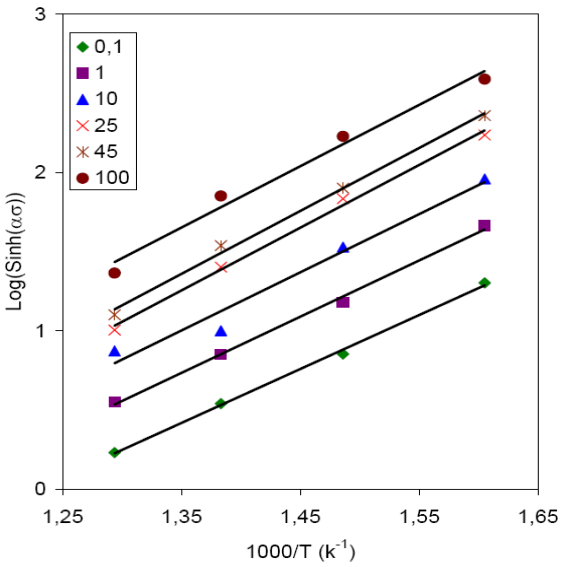

Figure 4- Plots of $\log\left(\sinh\left(\alpha\sigma\right)\right)$ against 1/T, at constant $\dot{\varepsilon}$ with α = 0.052 MPa^{-1}.

Table 5- Constitutive parameters of n, S and QHW of the AA7020 alloy variants used in this study.

n	S	Q_{HW} (kJ/mol)
3.74	2.19	156.9

4.2 FEM simulations

4.2.1 Validation of the predictions

Extrusion parameters predicted by FEM were used in the model in terms of strain, strain rate and temperature. Direct measurement of strain and strain rate or residual stress is beyond the scope of this article. The only parameter possible to be measured during experiments was the temperature at the surface of the extrudate at the die exit, which is a complex function of adiabatic heating depending on strain and strain rate and frictional heating depending on strain rate and interface tribological characteristics. Fig.

5 shows comparisons between the predicted and experimentally measured temperatures on the surfaces of the extrudates. The model predictions and experimental results have a maximum deviation of 5 % and thus are in reasonable agreement with experimental results.

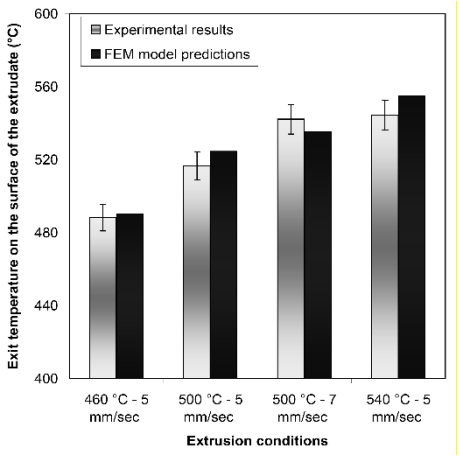

Fig. 5- Comparison between the predicted and experimentally measured temperatures at the surfaces of the extrudates.

4.2.2 Temperature profile in the peripheral part of the extrudate

The evolutions of temperature determined by tracking a point in the periphery part of the extrudates under different extrusion conditions till it reached the position of 500 mm away from the die orifice are shown in Fig. 6. It should be noted that these points may travel different distances before reaching to the die orifice. However, in order to keep similarity for all points, similar travel distance for all points is presented and the rest of the plot is deleted. It should be added that these data and those presented in Figs. 7 and 8 are extracted from a typical point at the periphery. The exact deformation history may slightly vary between other points at the periphery.

The peak in each of the temperature profiles corresponded to the moment when the tracking point left the die orifice where the material gained deformational heating and

frictional heating the most. Obviously, when a higher ram speed was applied, the tracking point left the extrusion die sooner. Therefore, the peaks in the temperature profiles at different ram speeds did not occur at the same time.

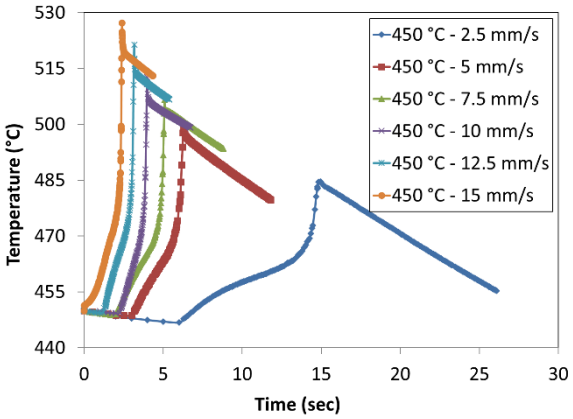

(a)

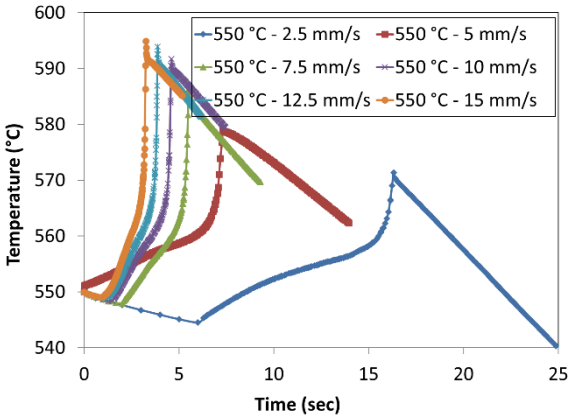

(b)

Figure 6- Evolution of temperature in the periphery of the extrudates at different ram speeds and billet temperatures of (a) 450 and (b) 550 °C.

It is well known that the peripheral part of the extrudate experiences higher temperatures as a combined result of severe deformation and friction between the workpiece and extrusion tooling. The amplitudes of temperature increase under different extrusion conditions, predicted from the present FEM simulations, were consistent with the validated values in the case of extruding other medium- and high-

strength aluminum alloys, i.e., AA6061 [20] and AA7075 [21]. Comparisons between the twelve extrusion runs at ram speeds of 2.5-15 mm/s and at the two billet temperatures, as shown in Fig. 6, showed that the temperature difference, i.e., the difference between the initial billet temperature and the maximum achieved during extrusion, was more significantly raised when the material was extruded at a higher ram speed and at a lower billet temperature. This may be correlated to a more significant adiabatic heating at low billet temperature and higher extrusion speed [3]. In fact, for a material with higher strength the adiabatic heating intensifies. When a lower billet temperature or higher strain rate is used, the material strengthen and more heat is generated during deformation and a more significant increase in temperature is observed. In addition, higher extrusion speed may limit the heat transfer time between the product and the die and environment, less heat is dissipated and consequently more heat increase may be observed.

4.2.3 Evolution of the effective strain in the peripheral part of the extrudate

The variations of the effective strain with time at a tracking point in the peripheral part of the extrudates under different extrusion conditions till it reached the position of 500 mm away from the die orifice are shown in Fig. 7. It is important to note that the effective strain itself was not a function of temperature, but its profiles (ie., the effective strain as a function of time) at different ram speeds and billet temperatures were not identical. There were no significant differences between the effective strain values under these extrusion conditions. The maximum strain occurred at the moment when the material left the die orifice. Obviously, the tracking point left the die orifice over a shorter period of time, when a higher ram speed was applied. For the particular die used in this study, the maximum effective strain was around 7-8.

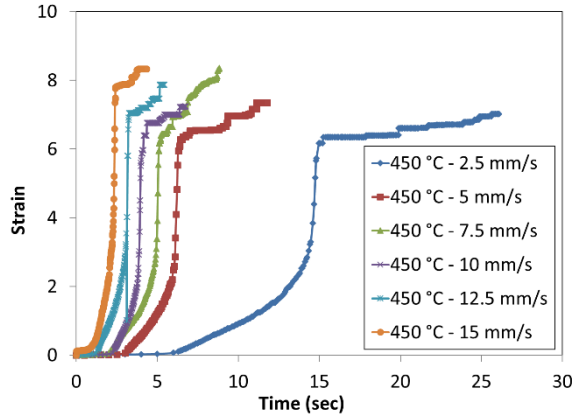

(a)

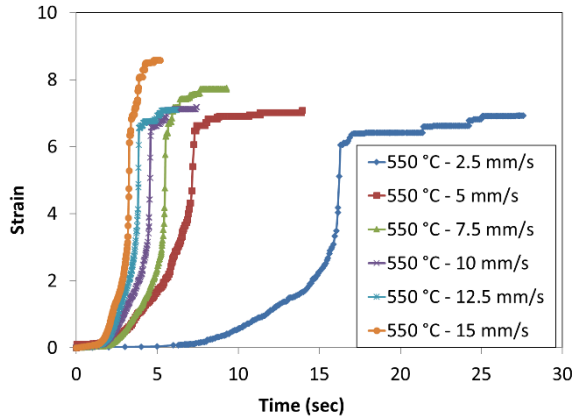

(b)

Figure 7- Evolution of the effective strain in the periphery of the extrudates at different ram speeds and billet temperatures of (a) 450 and (b) 550 °C.

4.2.4 Evolution of the effective strain rate in the peripheral part of the extrudate

The variations of the effective strain rate with time during extrusion under different conditions are shown in Fig. 8. It can be seen that the effective strain rate is higher at a higher ram speed. It is clear that at the highest ram speed of 15 mm/s, strain rate reaches 60 s^{-1}. In other FEM predictions, the highest value was found to be 75 s^{-1}, which was considered as the highest level used in the present compression tests.

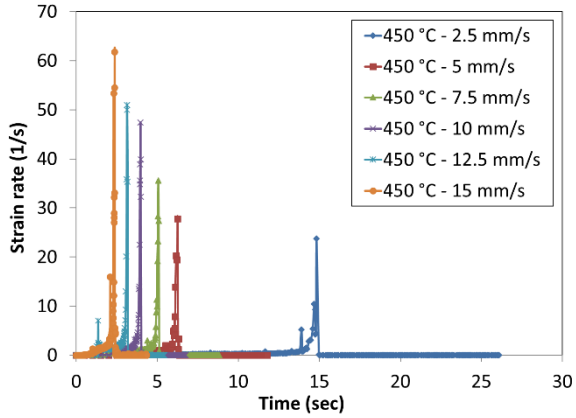

(a)

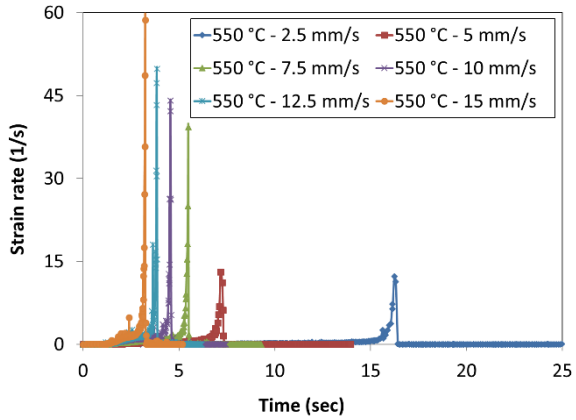

(b)

Figure 8- Evolutions of the effective strain rate in the peripheral of the extrudates at different ram speeds and billet temperatures of (a) 450 and (b) 550 °C.

4.2.5 Temperature increase in the peripheral part of the extrudate

It was indicated in section 4.2.2 that the data presented in Figs. 6 to 8 are extracted from a typical point at the periphery. However, the exact deformation history may slightly vary between other points at the periphery. Therefore, to facilitate the comparison between the predicted values of temperature under different extrusion conditions, the average temperature increases at three tracking points were extracted from the FEM simulation results, as shown in Fig. 9. It is clear that the amplitude of the temperature increase differed, depending on extrusion speed and billet temperature. The maximum temperature increase occurred when extrusion was performed at the lowest billet

temperature, i.e., 350 °C. With ram speed increasing up to 10 mm/s, the temperature increase became greater, which was attributed to a shorter period of time for heat transfer between the deforming material and the surrounding. However, with ram speed further increasing, the temperature increase tended to stabilize. Under the extrusion conditions used in the present FEM simulations, the average value of the temperature increase was 45 °C. However, a value of 75 °C or higher could be reached at a billet temperature of 350 or 400 °C and at a ram speed of 10 mm/s or higher. This value was considered representative of a harsh thermal condition occurring in the peripheral part of the extrudate and used in the design of physical simulations.

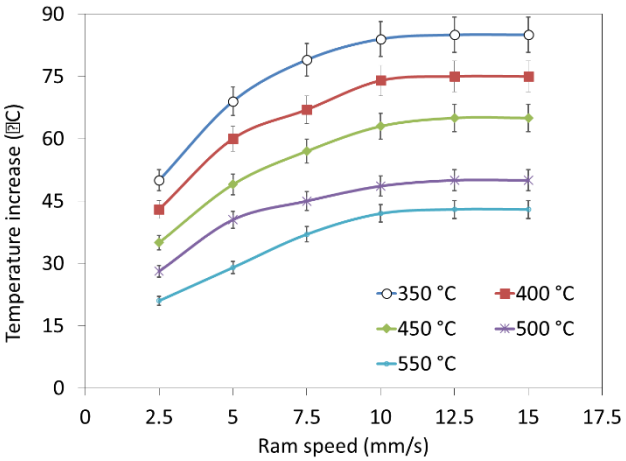

Figure 9- Temperature increase in the periphery of the extrudates at different ram speeds and billet temperatures.

4.1.5 Maximum effective strain rate in the peripheral part of the extrudate

The variations of the maximum effective strain rate in the peripheral part of the extrudates at different ram speeds and billet temperatures are shown in Fig. 10. A direct correlation between the maximum strain rate at the periphery of the extrudate and ram speed could be established. One may notice that the maximum effective strain rate

varied over a wide range between 15-80 s^{-1}. This variation of strain rate in the periphery of the extrudate is correlated to the various extrusion speeds.

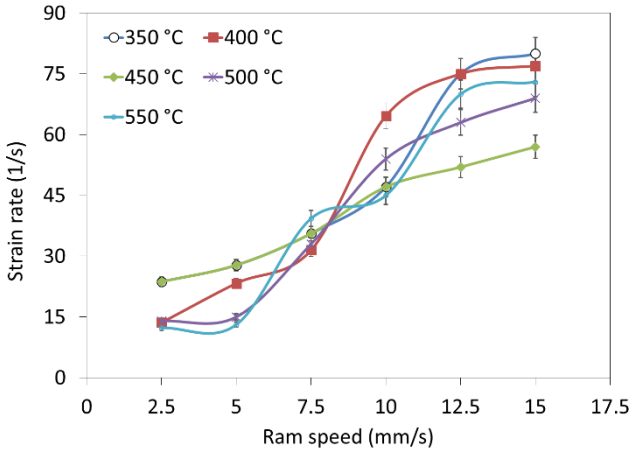

Figure 10- Variations of the maximum effective strain rate in the peripheral part of the extrudates at different ram speeds and billet temperatures.

4.1.6 Cooling time of the extrudate

As mentioned earlier, the quenching facility was placed at a distance of 1.25 m away from the die orifice. This means that the time during which the material was exposed to high temperatures before quenching, i.e., the cooling time, depended on the extrusion speed. In other words, recrystallization and grain growth could be stopped earlier when extrusion speed was higher. As presented in Fig. 11, the cooling time ranged between 5 and 30 s for the ram speeds used in the present investigation (2.5 – 15 mm/s). In the physical simulations, a holding time of 15 s at a representative increased temperature of 75 °C above the deformation temperature was chosen to represent the average cooling time after extrusion.

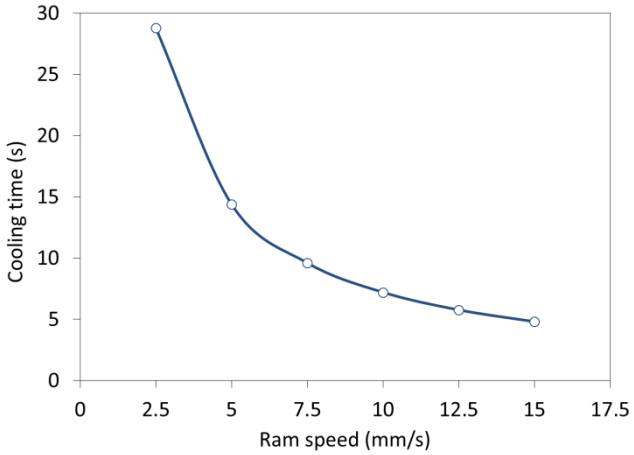

Figure 11- Variation of the cooling time with ram speed.

4.3 Microstructural evolution during and after hot compression tests

4.3.1 Grain structure of the sample prior to hot compression

Figure 12 shows the microstructure of the samples prior to hot compression test. It can be seen that the microstructure is composed of relatively coarse and equiaxed grain structure with an average size of 273µm. Formation of this microstructure may be attributed to the application of annealing after the hot extrusion process which was performed to reduce the effects of previous deformation. Different colors observed in this image has no specific meaning other than showing the fact that the grains with similar color have close orientations.

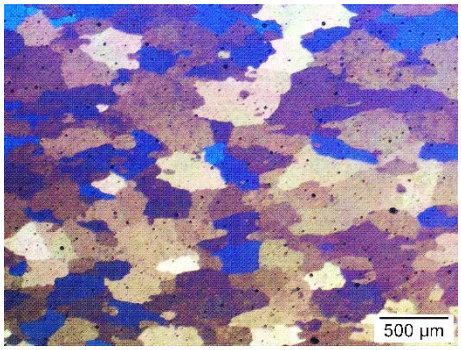

Figure 12- Initial microstructure of the sample

4.3.2 Grain structure of the alloy in the as-deformed state

Effect of deformation temperature at a strain rate of 75 s^{-1} on the grain structure of the specimens is shown in Fig. 13. The samples have been water-quenched after deformation to freeze microstructure. It can be seen that the matrix is in general deformed and many shear and deformation bands are observed in the microstructure. Indeed, these bands are observed in the form of parallel inclined lines throughout the microstructure. In addition, a few of recrystallized grains are observed being small and circular in shape. The fraction of recrystallized grains increases with deformation temperature. In fact, it changes from 12 to 17.5% as deformation temperature increases from 350 to 500 °C. The increase in the fraction recrystallized with increasing deformation temperature could be attributed to the increases in the mobility of grain boundaries at a higher temperature [12], which increases the growth rate of the nuclei and grains formed [12].

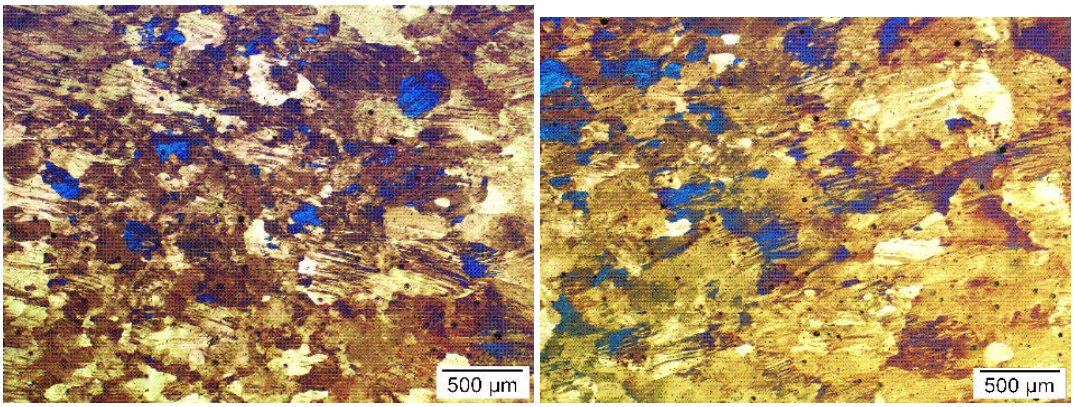

(a) (b)

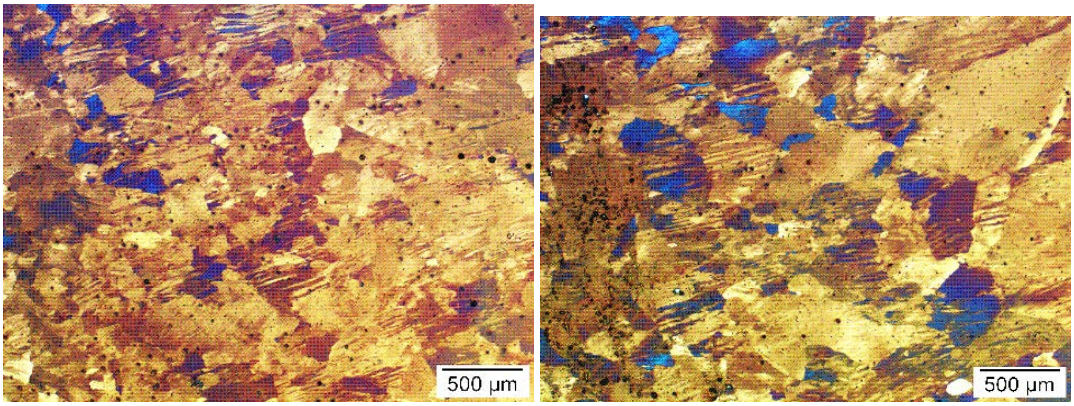

(c) (d)

Figure 13- Effect of deformation temperature: (a) 350, (b) 400, (c) 450 and (d) 500 °C on the grain structure of the specimens deformed at a strain rate of 75 s^{-1} and then water-quenched.

4.3.3 Effect of deformation temperature on grain structure after the special thermal treatment

As explained in experimental procedure, a special thermal treatment was applied on the samples in order to simulate the thermal history that the periphery of the extrudate go through. The effect of applying the especial thermal treatment on the microstructure and grain size distribution of the specimens deformed at a strain rate of 75 s^{-1} is shown in Fig. 14. The average grain size is as well presented on the graphs. It is clear that the average grain size increased with increasing deformation temperature. In addition, it can be observed that the grain structures are homogenous, regardless of deformation temperature. This might be because grain growth took place at similar rates and no abnormal grain growth occurred during the special thermal treatment [12].

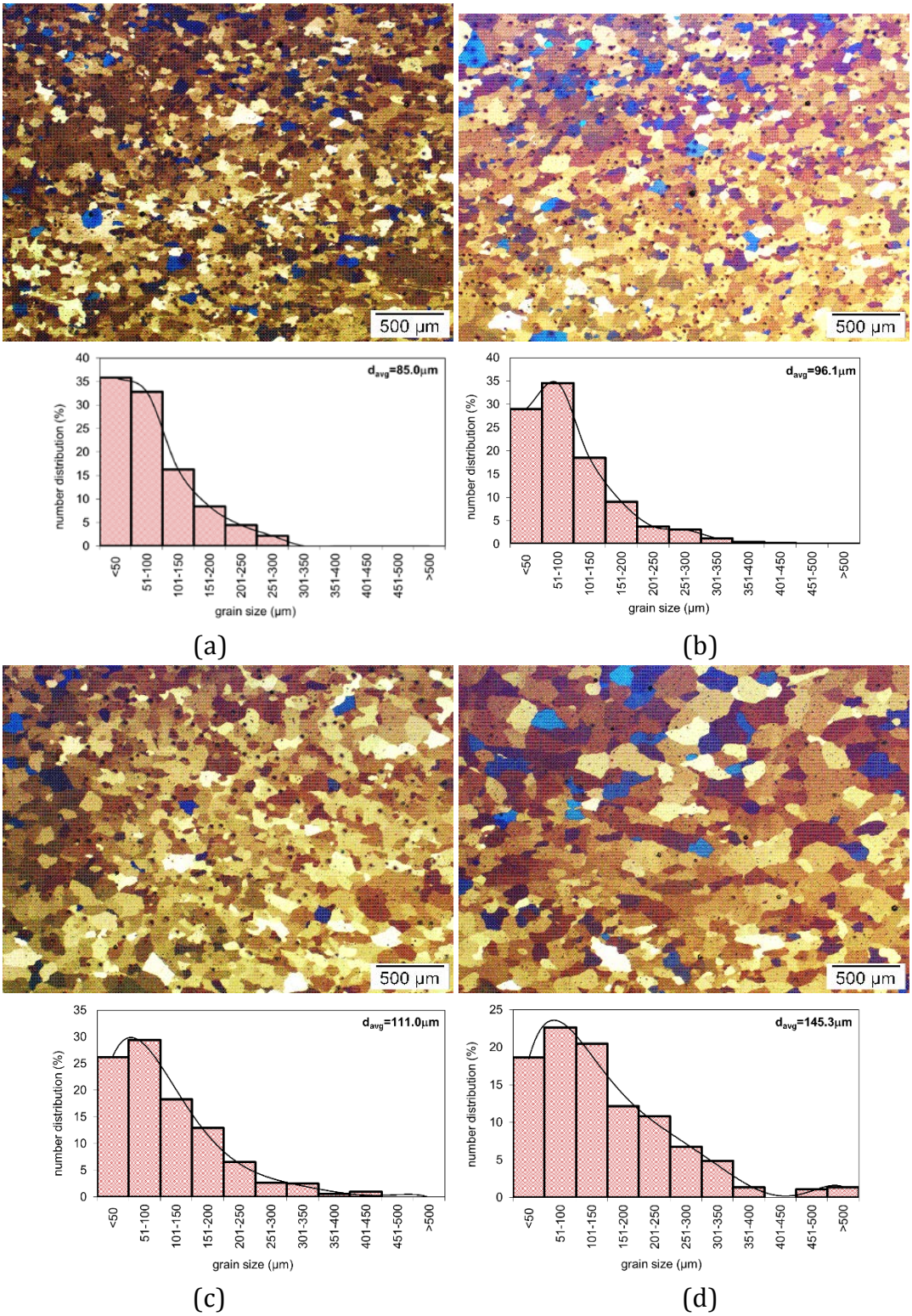

Figure 14- Effect of deformation temperature: (a) 350, (b) 400, (c) 450 and (d) 500 °C on the microstructure and grain size distribution of the specimens deformed at a strain rate of 75 s^{-1} and then subjected to the special thermal treatment.

4.3.4 Effects of strain rate on grain structure after the special thermal treatment

Fig. 15 shows the effect of special thermal treatment at different strain rates on the microstructure and grain size distribution of the specimens deformed at 500 °C. It can be seen that the sample deformed at 1 s^{-1} is partially recrystallized indicated by formation of a few fine and equiqaxed grains. In addition, a few number of shear bands indicating a deformed microstructure can be observed. The fraction of recrystallization increases and the grain size reduces as the strain rate increases. This may be due to increasing the number density of nucleation sites at higher ram speed [12]. In addition, more homogeneous grain size is achieved at a higher strain rate. If homogenous nucleation is assumed to occur, the stored energy is released through the formation of new grains [12], leading to a fully recrystallized grain structure. Newly formed grains tend to grow continuously at the same rate until they impinge each other. Afterwards, any further increases in grain size are not expected [12].

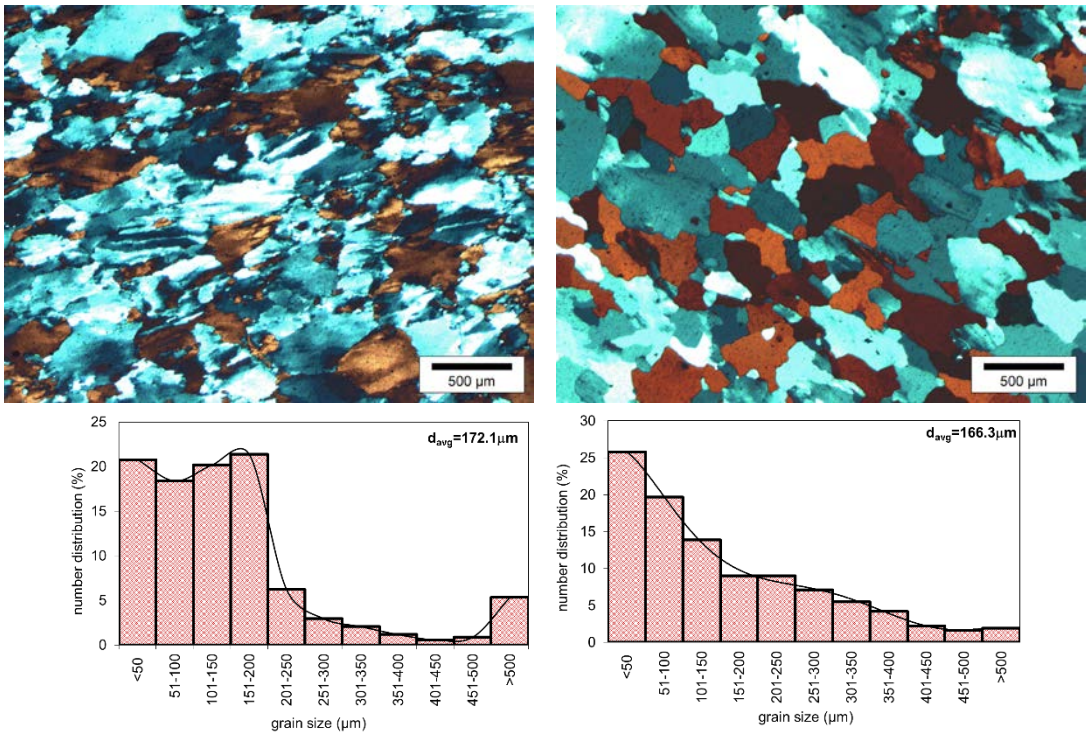

(a) (b)

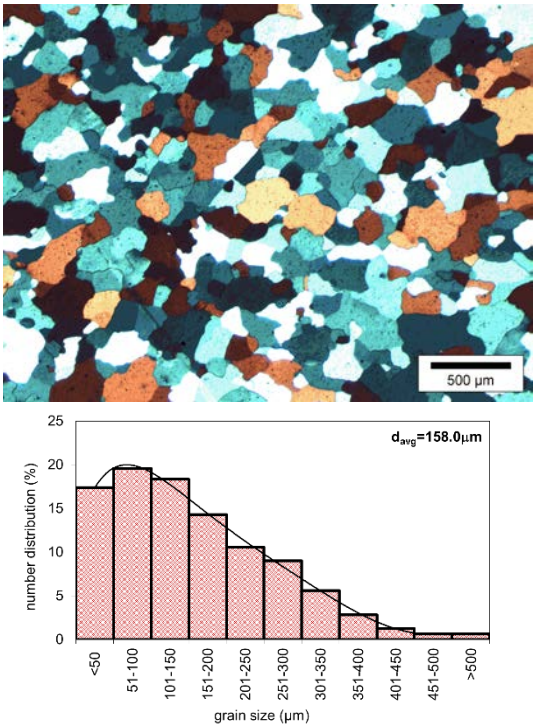

(d)

Figure 15- Effect of strain rate (a) 1, (b) 10, (c) 75 s^{-1} on the microstructure and the grain size distribution of the specimens deformed at 500 °C and then subjected to the special thermal treatment.

Decreased grain structure homogeneity at a lower strain rate may be attributed to a decrease in nucleation density. As deformation at a lower strain rate results in a lower stored energy in the material [12], nucleation may occur only in high-energy areas such as at grain boundaries and on large second-phase particles. Consequently, new grains will have large space to grow. The growth rate of the new grains depends on the orientation of the nuclei in the matrix [12] and the number of recrystallized grains in the region [12]. This results in different growth rates and eventually different grain sizes.

4.4 Formation of the PCG structure in the periphery of the extrudate

Fig. 16 shows the microstructure and grain size distribution in the periphery of a rod extruded at a temperature of 450 °C, extrusion speed of 3 m/min and at a reduction ratio of 15:1. The as-extruded microstructure was composed of large grains only. Analysis of the distribution of grain sizes showed that most of the grains were in the same size range. In other words, the homogeneity in grain size was remarkably high.

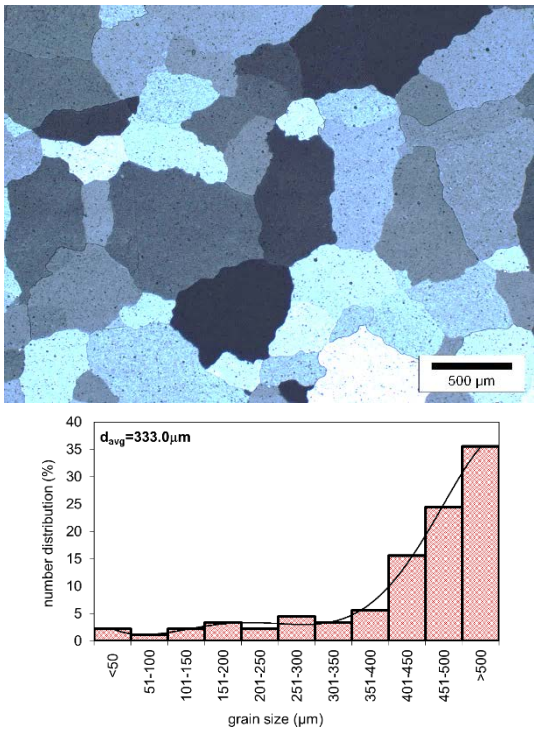

Figure 16- Microstructure and grain size distribution of the material extruded at a billet temperature of 450 °C, an extrusion speed of 3 m/min and a reduction ratio of 15.

It is important to separate the effect of strain rate on grain size from the effect of temperature. The results obtained from the FEM simulations (Fig. 8) have shown that in the peripheral part of the extrudate the effective strain rate can reach large values up to 45 s^{-1}. Due to strong shear deformation at such high strain rates and friction between the peripheral part of the workpiece and the extrusion die, the local temperature increases significantly. As discussed earlier, with increasing deformation temperature,

grain size increases. It has been also shown in Fig. 15 that higher strain rate results in a more homogenous recrystallized structure consisting of smaller grains. Therefore, it can be concluded that the coarse grain structure in the peripheral part of the extrudate is not a result of large strain rates. As shown in Fig. 1, grain size is strongly dependent on temperature. During extrusion, due to large strain rates and the friction between the workpiece material and the die, temperature increases and therefore, severe grain growth occurs. Therefore, relatively large recrystallized grains may be primarily due to high temperatures rather than to large strain rates. Therefore, in order to reduce the extent of the PCG structure, deformation temperature should be kept as low as possible, which can be achieved by applying forced cooling to the extrusion die [22].

One final point that needs to be clarified is that the maximum strain applied in hot compression tests in this investigation is 0.6. However, as shown in Fig. 7, the average effective strain in a routine extrusion process may be around 7-8. This may cause discrepancy between the results obtained from hot compression tests and a real extrusion process and should be taken into consideration.

5. Conclusions

According to the thermal history experienced at the surface of an extruded profile leading to peripheral coarse grain (PCG) structure, a special thermal treatment is proposed to be applied after hot compression testing. The effects of deformation conditions, i.e., temperature and strain rate, and the subsequent special thermal treatment on the formation of coarse grains in the AA7020 aluminum alloy are investigated and the following conclusions have been drawn;

1. Temperature increase at the periphery of an extrudate changes with initial billet temperature and ram speed. The temperature increase is higher for samples extruded at lower temperature and higher ram speed.
2. With increasing deformation temperature or decreasing strain rate, the average recrystallized grain size increases. Deformation temperature and the special thermal treatment representing the temperature increase during extrusion have insignificant effects on the homogeneity of the grain structure. However, with increasing strain rate, the homogeneity of the grain structure improves. Therefore, a fine and homogenous grain structure can be achieved by increasing strain rate.
3. The formation of coarse grains in the peripheral part of the extrudate is due to local high temperatures rather than high strain rates. In fact, with increasing billet temperature, or decreasing ram speed, the average recrystallized grain size increases. Therefore, a coarse grain structure in the periphery of the extrudate is not a direct result of large strain rates, because with increasing strain rate decreases in recrystallized grain size are normally expected.
4. Extrusion at a large strain rate results in significant increases in temperature and consequently increases in grain size due to high temperatures. To reduce the probability of the occurrence of the PCG structure, deformation temperature is recommended to be kept as low as possible.
5. The data and conclusions which have been presented in this investigation are derived based on hot compression tests in which the maximum applied effective strain is 0.6. However, in a routine extrusion process the effective strain may be around 7-8. This may cause discrepancy between the results obtained from hot

compression tests and a real extrusion process and should be taken into consideration.

6. References

[1] H. Zhang, G. Lin, D. Peng, L. Yang, Q. Lin, Dynamic and static softening behaviors of aluminum alloys during multistage hot deformation, Journal of materials processing technology, 148 (2004) 245-249.

[2] J. Luo, M. Li, D. Ma, Microstructure and mechanical properties of 7A09 aluminium alloy after isothermal compression and solution treatment, Journal of Materials Processing Technology, 212 (2012) 1039-1048.

[3] T. Sheppard, Extrusion of aluminium alloys, Springer, 1999.

[4] M. Schikorra, L. Donati, L. Tomesani, A. Tekkaya, Microstructure analysis of aluminum extrusion: Prediction of microstructure on AA6060 alloy, Journal of Materials Processing Technology, 201 (2008) 156-162.

[5] W. Misiolek, Material physical response in the extrusion process, Journal of materials processing technology, 60 (1996) 117-124.

[6] S. Kikuchi, H. Yamazaki, T. Otsuka, Peripheral-recrystallized structures formed in Al□Zn□Mg□Cu□Zr alloy materials during extrusion and their quenching sensitivity, Journal of materials processing technology, 38 (1993) 689-701.

[7] Y. Zhao, B. Song, J. Pei, C. Jia, B. Li, G. Linlin, Effect of deformation speed on the microstructure and mechanical properties of AA6063 during continuous extrusion process, Journal of Materials Processing Technology, (2013).

[8] J. Robinson, T. Liu, A. Khan, M. Pomeroy, Influence of processing on the properties of the aluminium alloy 2025 with a zirconium addition, Journal of Materials Processing Technology, 209 (2009) 3069-3078.

[9] J.H. Kim, J.H. Kim, J.T. Yeom, D.-G. Lee, S.G. Lim, N.K. Park, Effect of scandium content on the hot extrusion of Al–Zn–Mg–(Sc) alloy, Journal of materials processing technology, 187 (2007) 635-639.

[10] W. Van Geertruyden, W. Misiolek, Analysis of peripheral coarse grain recrystallization in 6xxx aluminum alloy extrusion, in: Proceedings of the 8th international aluminum extrusion technology seminar, 2004, pp. 107-113.

[11] P. Wang, W. Van Geertruyden, W. Misiolek, Formation of surface recrystallization of Al-Mg-Si alloy during extrusion, in: Materials Solutions Conference 2003, 2003.

[12] F.J. Humphreys, M. Hatherly, Recrystallization and related annealing phenomena, Elsevier, 1995.

[13] N. Parson, S. Barker, A. Shalanski, C. Jowett, Control of grain structure in Al–Mg–Si extrusions, in: Proceedings of the 8th international aluminum extrusion technology seminar, 2004, pp. 11-12.

[14] Eivani, A.R., Ahmed, H., Zhou, J., Duszczyk, J., The correlation between deformation conditions and peripheral coarse grain structure in extrusion of AA7020 aluminum alloy, 137th TMS Annual Meeting and Exhibition, 2008; New Orleans, LA; United States; 9 March 2008 through 13 March 2008. Pages 25-32.

[15] A.R. Eivani, Modeling of microstructural evolution during homogenization and simulation of transient state recrystallization leading to peripheral coarse grain

structure in extruded Al-4.5 Zn-1Mg alloy, in: PhD thesis Materials Science and Engineering, Delft University of Technology, Delft, The Netherlands, 2010.

[16] F. Slooff, J.B.J. Zhou, J. Duszczyk, L. Katgerman, Data Correction for Constitutive Analysis of Wrought Magnesium Alloys Based on Compression Tests, in: Proceedings of the 7th International Conference: Magnesium Alloys and Their Applications, Edited by KU Kainer, Verlag Wiley-VCH, Weinheim, 2007, pp. 324-329.

[17] ASTM standard, E112-96, in: Standard test methods for determining average grain size, ASTM standard, 2004.

[18] ASTM Standard, E562-89, Metallography, in: Non Destructive Testing, 1995.

[19] Cerri, E., et al., *Comparative hot workability of 7012 and 7075 alloys after different pretreatments.* Materials Science and Engineering: A, 1995. **197**(2): p. 181-198.

[20] T. Chanda, J. Zhou, L. Kowalski, J. Duszczyk, 3D FEM simulation of the thermal events during AA6061 aluminum extrusion, Scripta Materialia, 41 (1999) 195-202.

[21] L. Li, J. Zhou, J. Duszczyk, Prediction of temperature evolution during the extrusion of 7075 aluminium alloy at various ram speeds by means of 3D FEM simulation, Journal of materials processing technology, 145 (2004) 360-370.

[22] H. Weiland, Industrial Application of Recrystallization Control in Aluminum Products, in: Materials Science Forum, Trans Tech Publ, 2004, pp. 349-356.